Egyptian Journal of Chemistry

http://ejchem.journals.ekb.eg/

Investigation of A Novel Antimicrobial Chitosan Packaging Hydrogel Film Based On Azoloazine Derivative

Maha Sultan[a], Asmaa F. Kassem[b], Maysa E. Moharam[c], Ghada Taha[d*]

[a]*Packaging Materials Department, National Research Centre, 33 El Bohouth St. (former El Tahrir st.), Dokki, Giza, Egypt*
[b]*Chemistry of Natural and Microbial Products Department, National Research Centre, 33 El Bohouth St. (former El Tahrir st.), Dokki, Giza, Egypt*
[c]*Microbial Chemistry Department, National Research Centre, 33 El Bohouth St. (former El Tahrir st.), Dokki, Giza, Egypt*
[d]*Pre-treatment and Finishing of Cellulose-based Textiles Department, National Research Centre, 33 El Bohouth St. (former El Tahrir st.), Dokki, Giza, Egypt*

Abstract

The purpose of this work is to develop a novel active packaging chitosan hydrogel film (H17@CH) containing azoloazine derivatives as a novel antibacterial agent (11-(2-chlorobenzylidene)-6-(2-chlorophenyl)-6a, 7, 8, 9, 10, and 11-hexahydro-6H-benzo[b] (cyclohepta[e][1,4]thiazepine). The H17 revealed significant cell viability. H17 was added to chitosan in various quantities (100, 130, and 150μg). Significant cell viability was found in the H17. Chitosan was mixed with H17 in varying concentrations (100, 130, and 150 μg). Escherichia coli, Staphylococcus aureus, and Candida albicans are all susceptible to the antibacterial effects of the films. The films were evaluated using ATR-IR, XRD, XPS spectroscopy, and SEM-EDS. The maximum swelling ratio was 69.413.9 g/g for H17(100)@CH. The H17(150)@CH film had the lowest WVP at 15.601.52 g.mm. $kPa^{-1}.h^{-1}.m^{-2}$. Guggenheim-Anderson-de Boer, Peleg, and Smith were utilized to model the water vapor adsorption isotherms. All of the models were perfectly fitted.

Keywords: Chitosan, Azoloazine Derivative, Packaging Hydrogel Film.

1. Introduction

Traditional food maintenance processes such as cooling, fermentation, drying; freezing, utilizing preservatives like organic acids and their salts, and thermal processing are given less emphasis in the emerging packaging trend known as "active packaging." Active packaging tends to maintain a modified atmosphere environment and allows interaction between packaging materials and food [1-6].

Active packaging can perform a variety of tasks, including oxygen, moisture, or ethylene scavenging, ethanol, and taste emission, and antibacterial activities [7, 8]. Bactericidal films can be created by mixing synthetic or natural antimicrobial ingredients into films or by applying them directly on food and are among the most promising antimicrobials active packaging materials [9, 10]. Antimicrobial agents that can be classed as natural antimicrobial agents or synthetic ones depending on their origins are responsible for the antimicrobial properties of food packaging. Natural antimicrobial agents in active packaging include plant extracts [11], essential oils [2, 12], organic acids [13], bacteriocins [14], inorganic compounds [15-17], enzymes, and proteins [18-20].

The assessment of the antimicrobial activity of packaging materials employing differing approaches is becoming a crucial aspect of food security and economic application [2, 8, 21]. Antimicrobial agents extracted from natural sources have been produced because they are reasonably safe and easy to obtain [19, 22-26]. On the other hand, natural antimicrobial ingredients are in limited supply as food production and packaging need to increase. As a result, organic synthetic antimicrobial agents were created. Synthetic antimicrobial agents offer the potential to reduce costs and high activity over natural antimicrobial agents, but their toxicity is often higher. Researchers have a critical issue in developing antimicrobial treatments with high effectiveness and low toxicity.

Synthetic organic compounds, which mostly contain ethylene diamine tetra acetic acid (EDTA) [27, 28], fungicides [29-31], parabens [32, 33], and other chemicals, are the principal antibacterial components in food packaging. Vanillin is a synthetic antibacterial agent, which belongs to the aromatic hydrocarbon group. Furthermore, its inhibitory function against germs (such as bacteria, molds, and yeast) demonstrates its potential as a food preservative. Previously, vanillin derivatives were shown to possess antibacterial efficacy against *E. coli*, *S. aureus*, and *Pseudomonas aeruginosa*, as well as fungal suppression [23]. Films containing ethyl vanillin (EV) and chitosan (CS)/poly (vinyl alcohol) (PVA) were created. The films showed high antibacterial action against both *Escherichia coli* and S. *Staphylococcus aureus* germs [34].

Isothiazolinone is a strong biocide that is utilized as a preservative in a variety of food packaging industries [35, 36]. Many isothiazolinone derivatives, including methylchloroisothiazolinone (MCI), octylisothiazolinone (OIT), enzisothiazolinone (BIT), isothiazolinone, and 3-iodo-2-propynyl butyl carbamate (IPBC) and methylisothiazolinone (MI), have been widely employed as preservatives in a wide range of products [37]. Also, By reacting cycloheptanethione with haloketones or hydrazonoyl chlorides, a novel series of fused thiazolopyrimidines was created in a short amount of time with a high yield. Additionally, the reactions of bis(chlorobenzylidene)cycloheptan-1-one with o-aminothiophenol and heterocyclic amines led to the production of benzo[b]cyclohepta[e][1,4]thiazepine derivative and cycloheptapyrimidines fused with various azoles. Evaluation of the antibacterial activity of the products revealed that the majority of the derivatives occasionally outperformed the standard antibiotic in terms of strength [38].

The antibacterial, antifungal, antiprotozoal, and antiviral properties of the 1, 3, and 4-oxadiazole ring have been proven in various new compounds. Thus according to multiple researches, novel oxadiazole compounds exceed current antibiotics and other antimicrobial agents in terms of activity, indicating that their prospective as new treatments is quite promising [39].

Thus the goal of this study was to create chitosan hydrogel films containing (H17) as unique active packaging films. The cytotoxicity of H17 and the antimicrobial inhibitory function of H17-containing films were investigated. ATR-IR, XRD, XPS, and SEM/EDS were employed to depict the films. The performance of H17 was assessed in terms of physical swelling characteristics, water vapor permeability, and water vapor sorption isotherms. The *In-* vitro release research was investigated.

2. Materials and Methods

Chitosan and tripolyphosphate sodium salt (TPP) were delivered from Sigma Aldrich. All of the other reagents were used exactly as they were received by us.

2.1. Azoloazine Derivative Synthesize (H17)
According to Kassem and associates, (H17) was produced in two processes as an effective antimicrobial compound [38].
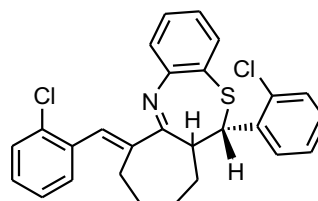
H17

2.2. Fabrication of chitosan hydrogel film
All chitosan hydrogel films were made using the solvent casting routine in the presence of (H17). To begin, chitosan (CH) (1g) solution was dissolved in 100 mL (1% acetic acid) and swirled until completely dissolved. CH was magnetically stirred for 15 minutes before being immersed in an ultrasonic bath for 30 minutes at 30 °C to achieve system homogeneity. The chitosan solution film was then cast in a Teflon Petri dish and allowed to dry at room temperature. The film was then soaked in tripolyphosphate sodium salt (TPP) cross-linker solution for 1 minute before being rinsed with distilled water and air dried. Furthermore, the technique was repeated using the above-described casting method with the antimicrobial component (H17) dissolved in ethanol (1mL) with different concentrations (100, 130, and 150 µg H17).

2.2. Characterization
2.2.1. ¹H NMR spectroscopy
The ^{1}H NMR spectrum of H17 was examined on a Bruker Advance 400 instrument at 400 MHz (JEOL, Tokyo, Japan) utilizing residual solvent signals as internal standards for ^{1}H-NMR in chloroform solutions.

2.2.2. Determination of cytotoxicity (MTT protocol)
The cytotoxicity of (H17) on the VERO cell line was investigated using salt MTT practice [40, 41].

2.2.2. Attenuated total reflectance infrared spectroscopy [ATR-IR] analysis

Fourier Transformation Spectroscopy (FTIR) of H17, CH, and H17@CH hydrogel films was achieved by the Attenuated Total Reflection (ATR) unit involved in FTIR-Vertex 70 Bruker, Germany (4000-400 cm^{-1}).

2.2.3. X-ray diffraction analysis (XRD)

The XRD analysis of H17, CH, and H17@CH hydrogel films was explored using a Bruker diffract meter (Bruker D 8 advance target). A CuK radiation source with a second monochromator (λ = 1.5405) could be used at 40 kV and 40 mA. The scanning rate for phase recognizing and line-broadening shape analysis was 0.2 per minute. According to equation (1) [2, 42], the crystallinity indices of CH and H17@CH hydrogel films were determined.

$$Crystallinity\ index\ \% = \frac{Intergrated\ area\ of\ crystalline\ peaks}{Total\ integrated\ area} \times 100 \dots\dots\dots\dots\dots\dots\dots (1)$$

2.2.4. X-ray photoelectron spectroscopy (XPS)

XPS of CH and H17@CH hydrogel films was achieved on K-ALPHA (Thermo Fisher Scientific, USA) with monochromatic X-ray Al K-alpha radiation -10 to 1350 eV spot size 400 micrometer at pressure 10-9 bar with full spectrum pass energy 200 eV and narrow spectrum pass energy 50 eV.

2.3.5. Surface morphology

SEM/EDS of CH and H17@CH hydrogel films utilizing SEM Model Quanta 250 FEG (Field Emission Gun) attached to EDX Unit (Energy Dispersive X-ray Analyses), with accelerating voltage 30 K.V., magnification 14x up to 1000000, and resolution for Gun.1n).

2.3.6. Swelling degree

Periodically, specimens of CH and H17@CH hydrogel films were pre-weighed and then immersed in a buffer solution (pH = 7.4). At fixed time intervals, the specimens were removed, cleaned with tissue paper to dispose of extra water, and then re-weighed yet again while gaining equilibrium. Equation (2) was employed to get the swelling degree (g/g) in which m_t refers to the specimen's weight at time (t), and m_o is the sample's initial weight [17, 43-46].

$$Swelling\ ratio = \frac{(m_t - m_o)}{m_o} \dots\dots\dots\dots\dots\dots (21)$$

A pseudo-second-order model was employed to explore the kinetics swelling of H17@CH with varying H17 content. Eq. (3) was utilized to estimate the swelling rate at (t), in which, W_t and W_e are swelling ratio at time (t) and at equilibrium. K is the rate constant [42, 43].

$$W_t = \frac{W_e^2 k_2 t}{W_e k_2 t + 1} \dots\dots\dots\dots\dots\dots\dots\dots (3)$$

Chi-square nonlinear error function (χ^2) as specified in (Eq.4) was used to determine the best-fitting model for capturing the investigational results with the analyzed swelling ratios, using data suited to theoretical, kinetic, high (R^2) and the lowermost (χ^2).

$$Chi - Square\ statistics\ (\chi2) = \sum \frac{(W_{c,\ exp} - W_c{'}_{fit})^2}{W_{c,}{'}_{fit}} \dots\dots\dots\dots\dots\dots (4)$$

2.3.7. Water vapor permeability (WVP)

The WVP of CH and H17@CH hydrogel films having varying H17 concentrations was determined gravimetrically using the modified ASTM E96-95, 1995 [47]. The polycarbonate bottles were pre-weighed and contained 10 g. of anhydrous calcium sulphates. The films, which had a diameter (6 cm) were inserted in polycarbonate bottles with parafilm around the circumference. The pre-weighed bottles were kept at 75 % relative humidity and 30 °C in a desiccator including a supersaturated solution of NaCl. For 12 hours, the WVTR was measured at a one-hour term. Each film was subjected to the same test. The weight gain of permeation bottles was used to assess the WVTR. Each film was subjected to the test three times. The bottle's weight change has been mentioned as a function of time.

The WVTR was measured via slope that was quantified with the support of a linear regression equation (Eq. 5). W_1 is the slope *(g/h.A)* is the film's exposed area (m^2). The correlation coefficients (R^2) should be ≥ 0.99.

$$WVTR = W_1\ \frac{1}{A} \dots\dots\dots\dots\dots\dots\dots\dots (5)$$

Water vapor permeability (WVP) (g. mm. m^{-2}. kPa^{-1}.h^{-1}) was determined as in (Eq. 6) [2, 42, 48, 49]. *While Pi and pa (25 °C) are the 75% relative humidity and air, respectively and L is the mean thickness (mm).*

$$WVP = L \times \frac{WVTR}{P_{i} - Pa} \dots\dots\dots\dots\dots\dots (6)$$

2.3.8. Determination of moisture sorption isotherm

Gravimetric analysis was used to investigate the effect of H17 content on the moisture sorption isotherms of chitosan and H17@chitosan hydrogel films. The specimens (30x30mm) have previously been dried for one day at 105°C. Prior to the insertion of the films in highly compact and sealed desiccators containing supersaturated salt solutions having differing relative humidity, the film samples were weighed. The experiment was carried out at 30 ºC. The samples were weighed at regular intervals until there was no weight change. All of the tested films' equilibrium moisture content (EMC) was calculated as g water/g dry film. Three times each sample was tested, with average

readings taken. The following formula (Eq.7) was used to estimate the EMC [2, 48, 49].

$$EMC = \frac{Final\ weight - Initial\ weight}{Initial\ weight} \quad \ldots\ldots\ldots\ldots (7)$$

2.3.8.1. Mathematical modeling of vapor isotherm

GAB (Eq. 8), Peleg models (Eq. 9), and Smith (Eq. 10) models, respectively were employed to represent the experimental data.

Where M_c stands for equilibrium moisture content, M_o for maximum moisture monolayer coverage capacity, and a_w for water activity; the constants of adsorption energy C and K stand for the energy interactions between the first and the next adsorbed molecules at specifically sorption sites [46, 50].

$$M_e = \frac{M_o CK\ a_w}{(1 - Ka_w)\ (1 - Ka_w + CK\ a_w)} \quad \ldots\ldots\ldots\ldots (8)$$

The Peleg model is an empirical one that has no fundamental assumptions background Equation (9) [51].

$$M_c = k1\ a_w^{N1} + k2\ a_w^{N2} \quad \ldots\ldots\ldots\ldots\ldots\ldots (9)$$

$k1$ is a mass transfer constant in this model; the lower $k1$, the higher the initial water adsorption rate; and $k2$ is a maximum water adsorption capability constant in this model; the lower $k2$, the greater the adsorption capacity [52, 53].

The Smith model (10) [54, 55].

$$M_c = A + B\ ln(1 - a_w) \quad \ldots\ldots\ldots\ldots\ldots\ldots (10)$$

The amount of water in the first sorbed fraction is A, and the amount of water in the multilayer moisture fraction is B.

2.3.9. Assay for antimicrobial potency

Foodborne Gram Negative and Gram Positive Bacteria and pathogenic yeast were assigned to test of antimicrobial potency of H17@chitosan hydrogel films (ATCC 10231). Qualitative valuation has been carried out on nutrient agar medium. At 37°C, the seeded plates were incubated for 24 hours. The inhibitory zones (IZ) were likely estimated (mm) [17].

2.4. Statistical Analysis

At least three duplicates of each experiment were carried out. The outcomes were displayed as mean standard deviation (±SD) and ANOVA test using the "SPSS" application. Duncan multiple comparison tests were performed to investigate the significant differences between the samples. Means with identical letters in each column signify that there is no statistical difference ($p < 0.05$).

3. Results and discussion

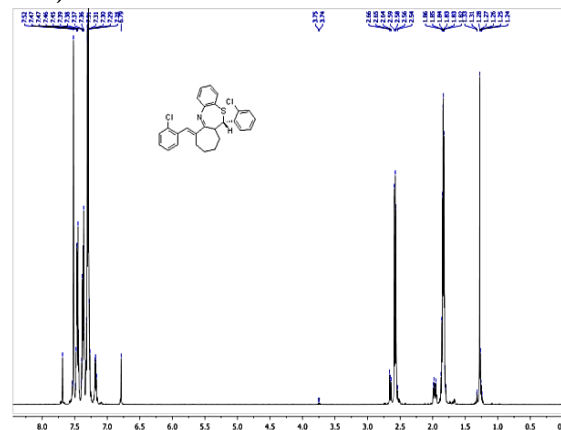### 3.1. Hydrogen Proton Magnetic Resonance (^{1}H NMR)

Figure 1: ^{1}H NMR H17.

In order to verify the possible structure of (H17), ^{1}H NMR technique was utilized. Figure (1) shows the ^{1}H NMR spectrum of H17. It was found 1.24-1.27(m,2H, CH$_2$), 1.82-1.86(m,2H, CH$_2$), 1.93-2.03(m,2H, CH$_2$), 2.56-2.59 (t,2H, J = 4.3Hz, CH$_2$), 2.64-2.69(t,2H, J = 4.1 Hz, CH$_2$), 3.74-3.75(d,2H, J = 4 Hz, CH$_2$), 6.79 (s, 1H, =CH), 7.17- 7.19 (m, 2H, Ar-H), 7.27- 7.32 (m,3 H, Ar-H), 7.32- 7.39 (m, 3H, Ar-H), 7.44- 7.48 (m, 2H, Ar-H), 7.57- 7.58 (d, 1H, J = 4.4 Hz, Ar-H), 7.71- 7.72 (d, 1H, J = 3.6 Hz, Ar-H) [38].
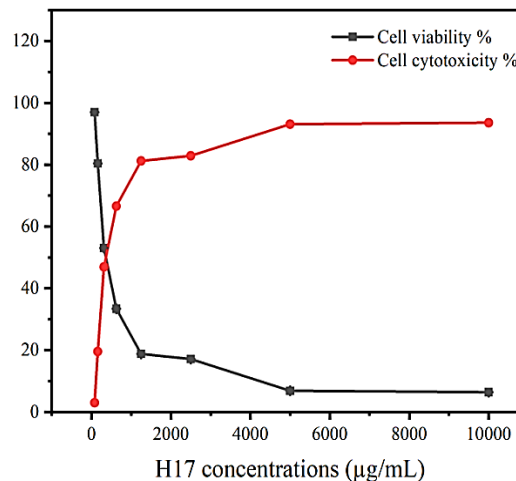
3.2. Cytotoxicity

Figure 2: Viability and cytotoxicity of H17 at diverse concentrations.

The cellular metabolic activity is usually measured by MTT assay which reflects the proliferation, survival, and cytotoxicity of cells. In the MTT assay, a yellow tetrazolium salt (3-(4,5-dimethylthiazol-2-yl)-2,5-diphenyltetrazolium bromide or MTT) is metabolically reduced by NAD(P)H-dependent oxidoreductase enzymes to formazan crystals (purple color) by active cells [56, 57]. The insoluble formazan

is dissolved in DMSO solvent and then spectrophotometrically measured at an absorbance of 500-600 nanometers. The darker the solution, the more live, metabolically active cells there are. The effect of diverse H17 concentrations on viability and cytotoxicity % of VERO cell-line was shown in Figure 2. The viability and cytotoxicity percentages are significantly dependent on the concentration of H17. When the concentration of H17 increased, the viability% decreased and at the same cytotoxicity increased. At concentration (150 µg), the viability and cytotoxicity percentages were 80.41 and 19.58 %, respectively. This indicates that H17 has a fair cytotoxicity at that concentration.

3.3. Attenuated Total Reflectance Infrared Spectroscopy (ATR-IR)

The ATR-IR spectra of (H17), chitosan (CH), and H17@CH hydrogel films were demonstrated in Figure (3). The ATR-IR spectrum of H17 shows a peak at 3055 cm^{-1} caused by the C-H stretching vibration of the benzene ring =C-H. The overlapping stretching vibrations of -C=C of the benzene ring and –C=N of the thiazepine ring of the H17 compound are represented by the strong band at 1663 cm^{-1}. The symmetrical and asymmetrical C-H stretching vibrations produce the strong two peaks at 2916 and 2884 cm^{-1}. The chorlobenzene ring's finger print region was 1500-400 cm^{-1}. The peaks at 867-538 cm^{-1} are caused by the chlorobenzene ring's –C-Cl.
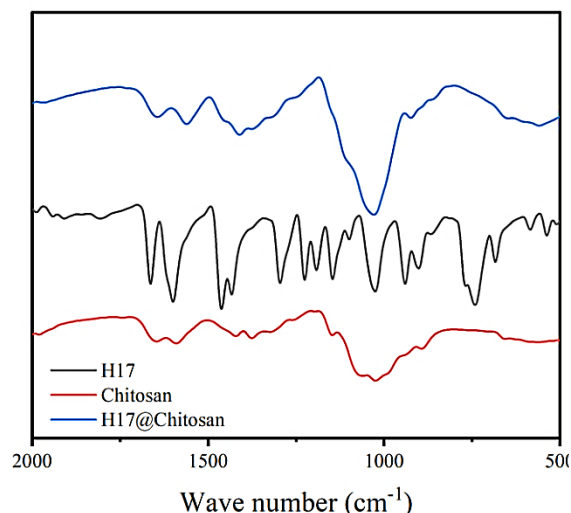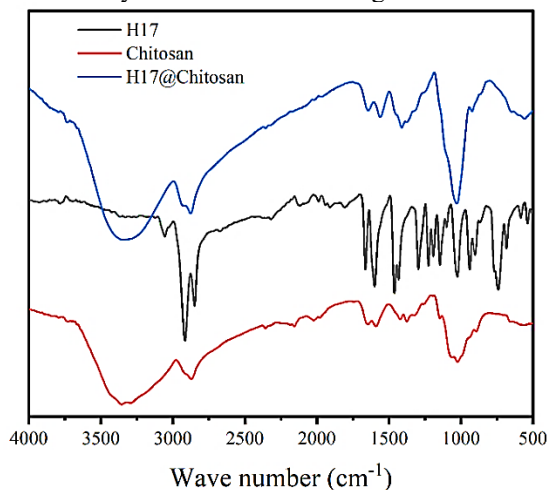

Figure 3: ATR-IR spectra of H17, CH, and H17@CH hydrogel films.

The chitosan shows a band at 2935 cm^{-1} that was attributed to methylene CH$_2$. The peak at 1734 cm^{-1} was referred to the C=O functional group of residual carbonyl and the peak at 1430 cm^{-1} was attributed to CH$_2$ bending vibration. In addition, the sharp absorption peak at 1030 cm^{-1} was assigned to C-O stretching. Moreover, the peak at 3350 cm^{-1} was related to O-H/-NH stretching. For H17@CH hydrogel film showed peaks at 2918, 2851, and 1665 cm^{-1} which corresponded to symmetrical and a symmetrical C-H stretching vibration, overlapped stretching vibrations of -C=C of the benzene ring, and –C=N of thiazepine ring of H$_{17}$ compound, respectively. The peaks at 3472, 1736, 1033 cm^{-1}, and 1224 cm^{-1} are assigned to –OH, -C=O, -O-C, and -C–O-C of chitosan, respectively. Moreover, the peaks that appear in the region of 867-538 cm^{-1} are due to –C-Cl of the chlorobenzene ring. This indicates the good incorporation of H17 into the chitosan hydrogel film.
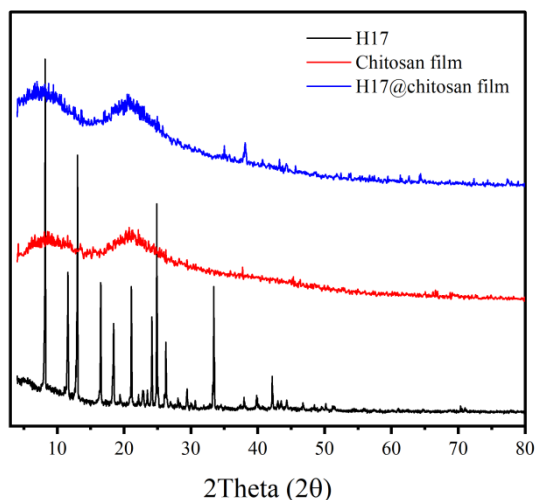
3.4. X-ray diffraction analysis (XRD)

Figure 4: XRD analysis of H17, CH, and H17@CH hydrogel films.

The XRD of H17, CH, and H17@CH hydrogel films are elucidated in Figure (4). It is shown that the diffractogram of chitosan is rather crystalline, it includes two peaks at 2Theta = $8.5°$ and $20.91°$. On the other hand, H17 is a highly crystalline substance. The H17@CH hydrogel film revealed multiple distinct peaks characteristic of H17 at 2Theta = 8.73, $2°.68°$, $31.03°$, $32.09°$, $36.02°$, $46.20°$, $54.0°$, $64.43°$, and $72.27°$. The addition of H17 to chitosan hydrogel film raises the crystallinity index percent. The crystallinity indices of CH hydrogel and H17@CH hydrogel films were 35.46% and 66.66%, respectively. This increase in the crystallinity index percent of the H17@CH hydrogel film is proof of its successful incorporation of H17 into chitosan hydrogel film.

3.4. X-ray photoelectron spectroscopy analysis (XPS)

PS spectroscopy would also quantitatively be used to explore the surface`s elemental analysis state. A comprehensive survey of CH and H17@CH hydrogel films is shown in Figure (5). Peaks at 286.29, 533.7, and 403.87 eV in the spectra of CH hydrogel correspond to C, O, and N with atomic ratio percentages of 74.44, 25.15, and 0.41 %, respectively. On the other hand, the H17@CH hydrogel film reveals new expected peaks that correlate to Cl and S. Peaks for C, N, O, S, and Cl with atomic percentages of 73.02, 3.541, 22.71, 0.71, and 0.02 % emerge at 286.5, 400.94, 533.97, 165.02, and 199.08 eV. The hydrocarbon (C-H/C-C), alcohol/ether/amine (C-NH/C-OH/C-O), and acetal (O-C-O) peaks in the C1s spectra of CH hydrogel film have binding energies of 284.25, 287.43, and 289.41 eV, respectively. However, three peaks at 284.98, 286.44, and 287.85 eV in the H17@CH hydrogel film could be agreed to C-H/C-C/ C=C and C-S/C-N/C-Cl, respectively [58, 59]. When compared to CH hydrogel film, the atomic ratio of the subpeak of H17@CH hydrogel film assigned to C-C increases from 56.85 to 76.48 percent. This is due to the benzene ring of H17 being incorporated into the CH hydrogel film with an extra -C=C-. The peaks at 401.68 eV matching the assignments of -NH were found in the N1s area of the XPS spectra of chitosan. However, two peaks at 399.58 and 401.73 in the H17@CH hydrogel film are attributed to C-NH/C-N=C [42, 44]. In the O1s region, C-O, and N-C=O were given by 533.11 and 530.32 eV. The peak at 534.56 eV could be caused by H_2O adsorbed on the CH hydrogel film surface. However, the O1s peaks in the spectra of H17@CH hydrogel films are virtually identical to CH but with a minor shift, C-O (533.01 eV), N-C=O (531.69 eV) and adsorbed water (534.12 eV), respectively [60]. The H17@CH hydrogel exhibits clear two Cl 2p peaks at 200.4 eV and 197.43 eV of atomic ratio present 75.62 and 22.13%, respectively that may be attributed to C-Cl. Another peak occurs at 198.0 eV, it is rather than likely contaminating species peaks for Cl [61]. H17@chitosan hydrogel, on the other hand, shows a peak at 163.7 eV, which corresponds to the–C–S–C– covalent bond [44, 62].
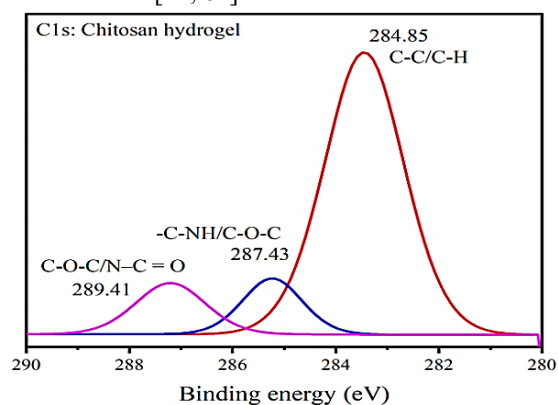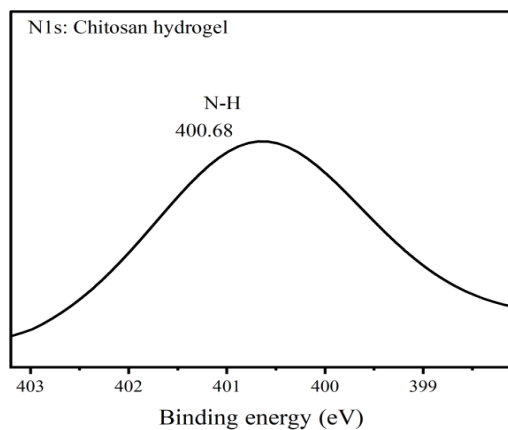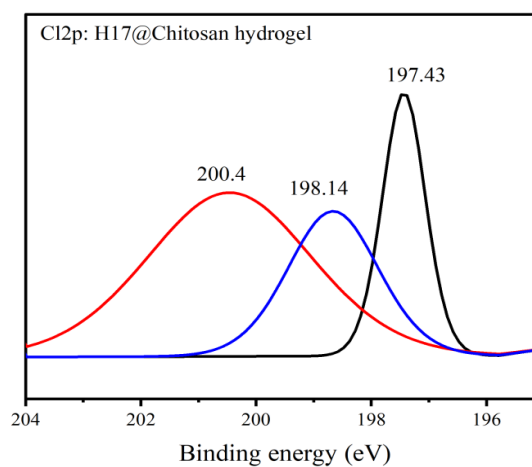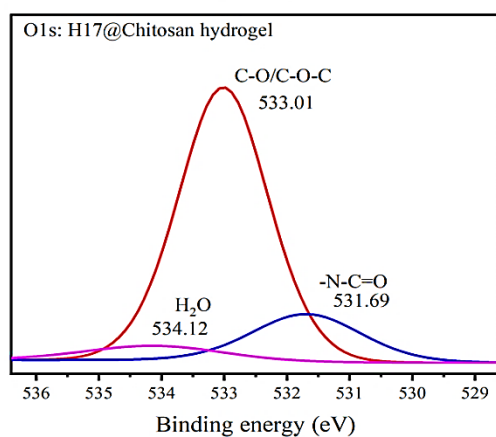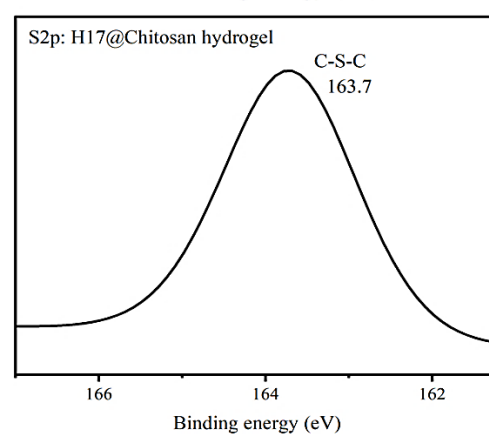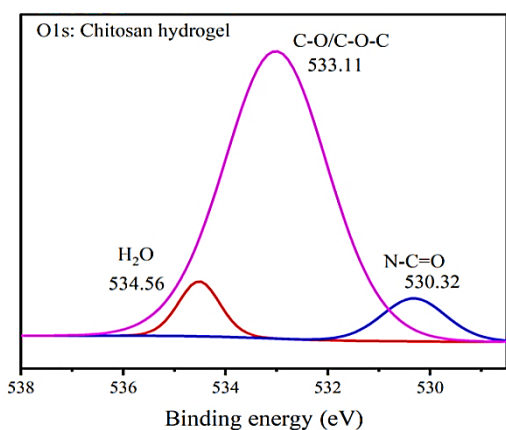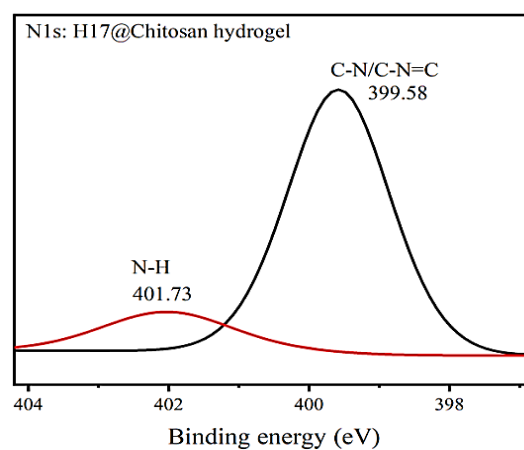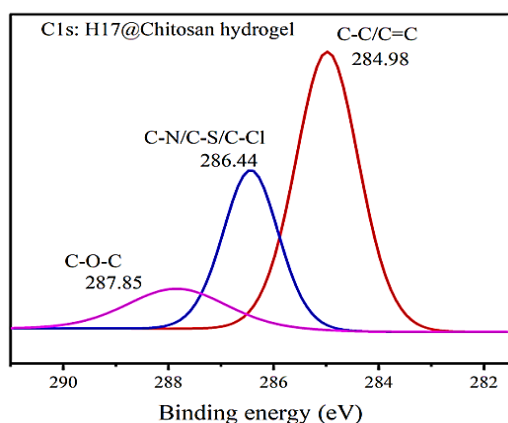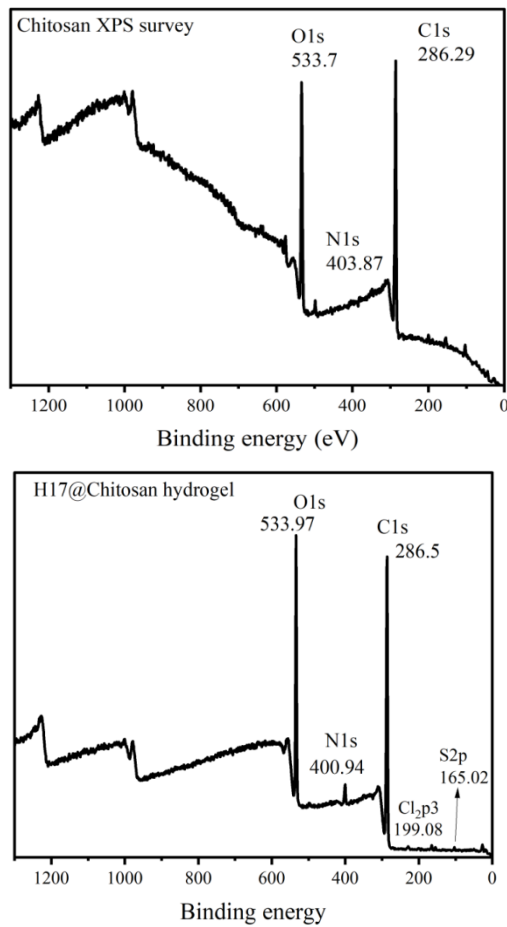
Figure 5: High resolution C1s, O1s, N1s ,Cl 2p, S2p XPS spectra of CH and H17@CH hydrogel

Figure 6: SEM images of (A) CH and (B) H17@CH hydrogel films and their EDS spectra.

3.5. Surface morphology (FE-SEM)

FE-SEM has been used to scan the obtained CH and H17@CH hydrogels. Figure (6) shows the morphology of the hydrogels, as well as an SEM study of the surface morphology. The hydrogel possesses tight, dense, and rough morphology, indicating its great toughness and dense cross-linking. This surface's roughness has a potential advantage, it will be more convenient to increase the surface area and will aid in the diffusion of water flow into polymer chains. The successful embedding of H17 into CH hydrogel is seen in the EDS spectra of CH and H17@CH hydrogels. The EDS spectrum of H17@CH hydrogel revealed the elemental composition of H17, which included C, O, N, Cl, and S.

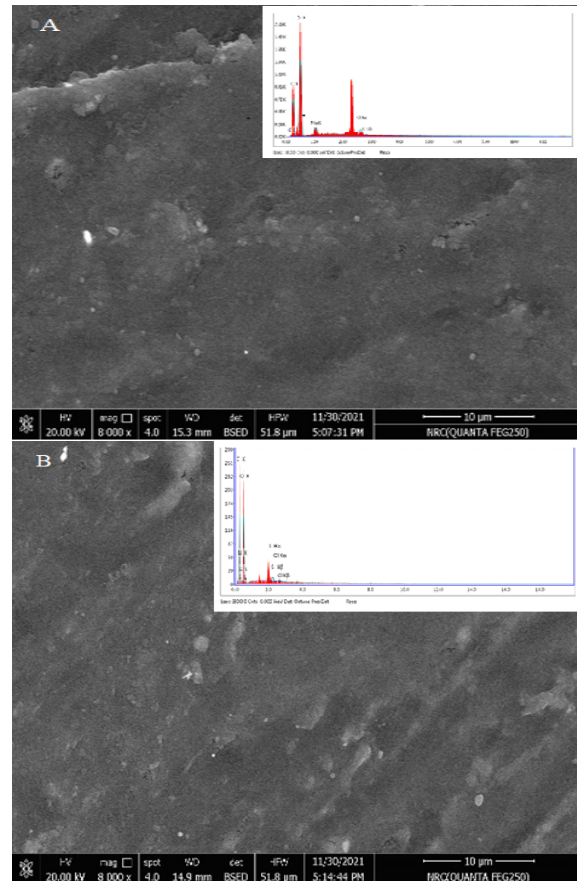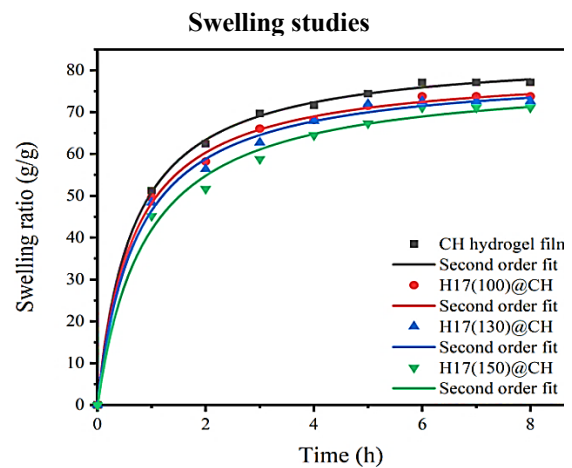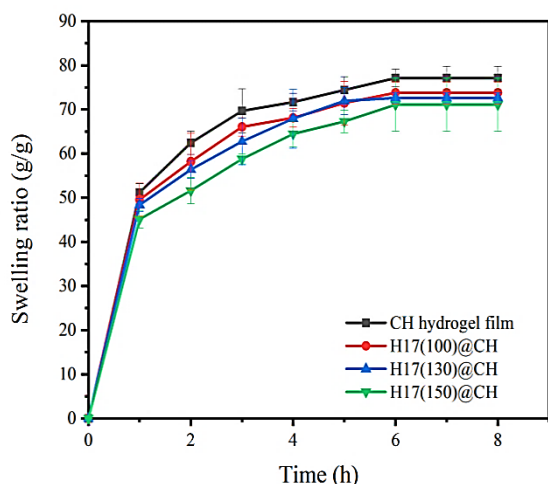Figure 7: Swelling ratio of CH and H17@CH hydrogel films containing different concentrations of H17.

The degree of swelling of CH and H17@CH hydrogel films is particularly fascinating. As a promising foundation for fine-tuning film properties, H17 increasing content was effectively determined to impact swelling degree. Swelling percentages decreased when H17 concentrations increased this can be attributed to the lipophilic nature of the heterocyclic organic compounds [46]. As a result, the more H17 in the film, the less water can diffuse into the polymer network. Figure (7) shows the swelling degrees versus time for H17@CH hydrogel films with H17 content at 25°C and a pH (7.4) buffer solution (6). The results reveal that as the H17 level increases, the equilibrium swelling degree decreases. The swelling ratios for H17(100)@CH, H17(130) @CH, and H17(150)@CH were 73.10± 2.5, 72.62± 1.1, and 71.07± 6.0 g/g, respectively compared with CH hydrogel film 77.11± 2.6 g/g.

Table 1: Swelling kinetics of H17@CH hydrogel films of different content.

Nonlinear Pseudo-second order					
Parameters	W_e exp (g/g)	W_e fit (g/g)	k ×10^{-3} (h^{-1})	R^2	χ^2
CH	77.11± 2.6	84.23±0.62	0.1803±9.19	0.9992	0.545
H17(100)@CH	73.10± 2.5	80.52±0.99	0.185± 1.5×10^{-3}	0.9978	0.35
H17(130)@CH	72.62± 1.1	80.11± 1.64	0.173± 2.01×10^{-3}	0.9957	0.66
H17(150)@CH	71.07±6.0	79.17±2.0	0.142± 2.13×10^{-3}	0.9925	0.45

The practical outcomes, as shown in Figure (7), were more in line with the hypothetical one. Modeling swelling kinetic characteristics of H17@CH hydrogel films were provided in Table (1). Higher correlation coefficients ($R^2 \geq 0.999$) were observed in Table (1) indicating a good matching with real swelling results. With the experimental swelling data (W_e) of 77.11±2.6, 73.10± 2.5, 72.62± 1.1, and 71.07± 6.0 g/g, the fitted W_e values were 84.23±0.62, 80.52±0.99, 80.11± 1.4, and 79.17± 2.0 g/g (Table 1).

3.6. Water vapor permeability
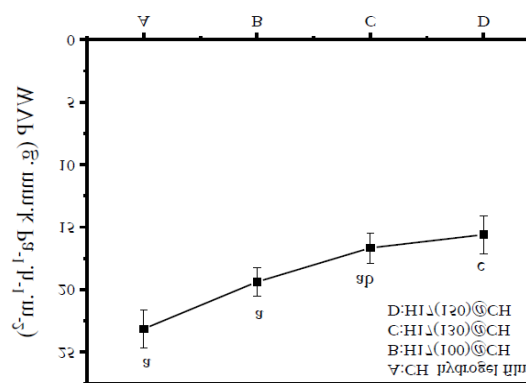
Figure 8: WVP of CH and H17@CH hydrogel films containing different concentrations of H17.

a-c: Means with identical letters signify that there is no statistical difference ($p < 0.05$).

The ability of a film to permit water gases to travel through it is referred to as "water vapor permeability" (WVP). H17@CH film serves as a shield between the product and its surroundings, preventing dehydration [36]. Figure (8) displays the WVP of H17@CH in
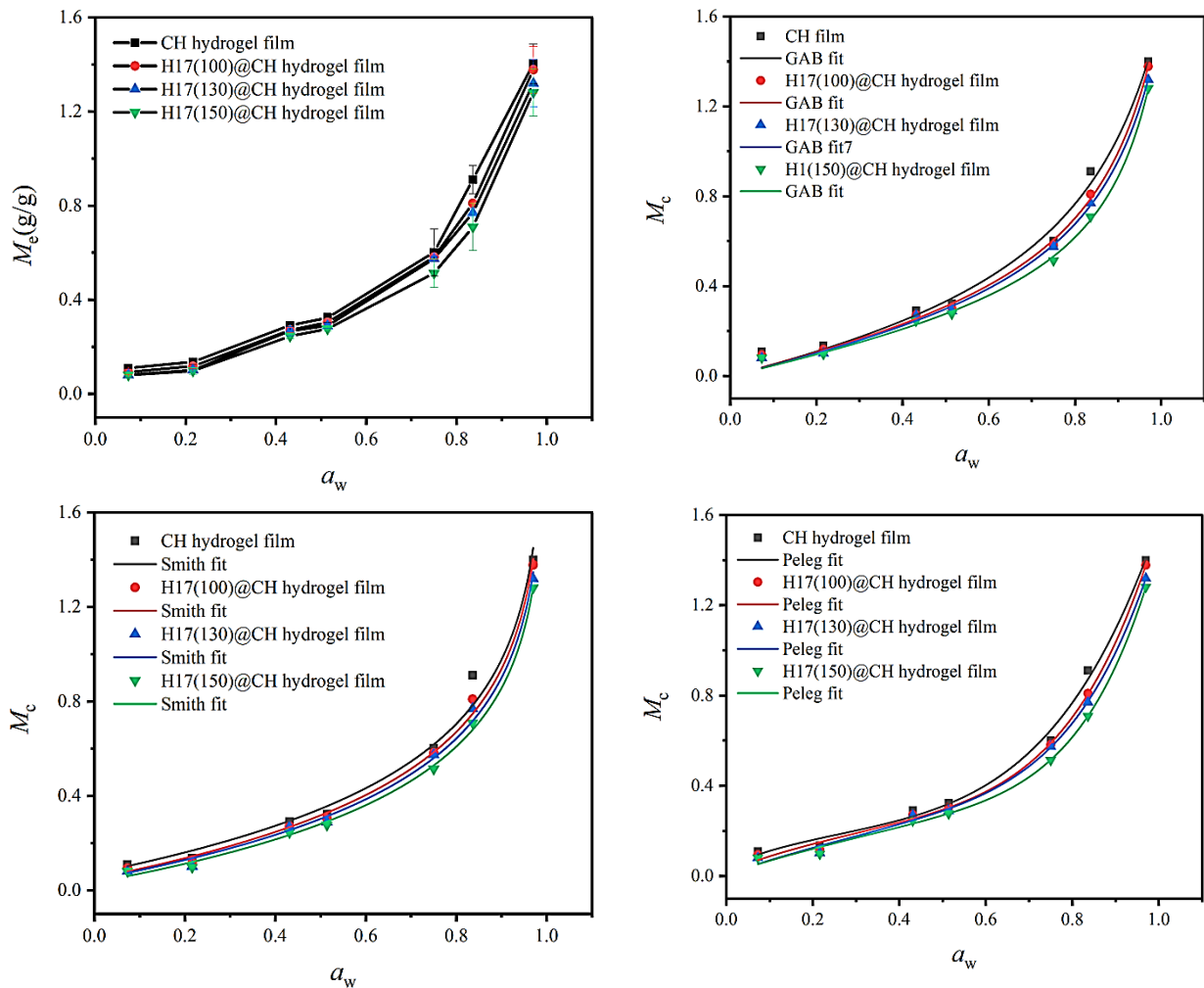
Figure 8: Equilibrium moisture content and fitting practical data of CH and H17@CH hydrogel films using GAB, Peleg, and Smith models.

combination with various H17 dosages. While H17 concentration increases, the WVP declines. Figure (8) shows that when compared to the CH control film, which had a WVP value of 23.14±1.52 g. mm.k Pa⁻¹.h⁻¹.m⁻², the H17(150)@CH film had the lowest WVP value (15.60±1.52 g. mm.k Pa⁻¹.h⁻¹.m⁻²).

3.8. Water vapor sorption isotherms

Packaging materials' moisture sorption aspects are widely employed to tune stable, long-term, and better-useable film for packaging purposes. Figure (9) depicts the equilibrium moisture sorption isotherms of H17@CH hydrogel films with various H17 contents (w/w) in comparison with CH hydrogel at 25 °C. The findings also revealed that when the H17 content increased, the equilibrium moisture contents (M_c) for each H17@CH hydrogel film reduced at the same a_w, implying that H17@CH hydrogel films are getting less hygroscopic. H17(100)(@CH), H17(130)(@CH), and

H17(150)(@CH hydrogel films had M_c (g/g) values of 1.378±0.10, 1.320±0.10, and 1.281±0.10 g/g dry, respectively, compared to CH hydrogel film 1.402±0.08 g/g dry. This decrease in M_c of H17@CH hydrogel films could be related to an increase in hydrophobicity of H17@CH hydrogel films due to the higher amount of novel antibacterial azoloazine derivatives agent H17 contained, resulting in less accessible polar groups. Similarly, the emergence of dense cross-linked regions of H17@CH hydrogel films leads into declining of the available water-binding sites [63].

3.8.1. Mathematical modeling of vapor isotherm
The purpose of this study was to see how different H17 concentrations in H17@CH film alter the water sorption isotherms of the H17@CH films. According to the GAB model [42], sorbate molecules in the second layer have the same state as those in superior layers but are distinct from those in the liquid state.

The monolayer value shows how much water may be bound to a single layer of dry film per gram. The monolayer (M_o) value is important because it represents the amount of water that is heavily adsorbed in certain locations and is regarded to be an indicator of packaging film stability. The monolayer moisture content is significantly affected by increasing H17 concentration in H17@CH hydrogel films. As the H17 concentration increases, M_o decreases. The more H17 there was, the less active site there was to bind water molecules, according to theory. In comparison to the CH hydrogel control film (1.870±1.016 g/g dry solids), the monolayer moisture contents of H17(100)@CH, H17(30mg)@CH, and H17(150)@CH were 1.637±1.059, 1.574±0.8605, and 1.283±1.391g/g, respectively, as shown in Table (2).

In the GAB models, C, is as well as, relevant to monolayer heat sorption, [55]. The difference in heat of sorption between a monolayer (E_1) and a multilayer (E_L) or bulk water is proportional to C [64]. This energy constant's high value proposes that water molecules are more firmly adsorbed in the matrix's active areas. The parameter C value dropped when CH hydrogel film was compared to various concentrations of H17, showing that this novel hydrophobic antimicrobial agent may reduce the portion of the polymer's sorption sites, as shown in Table (2). H17(100)@CH, H17(130)@CH, and H17(150)@CH had C parameter values of 0.403±0.404, 0.344±0.1569, and 0.339±0.1809, respectively compared with CH control sample (0.4704±0.430).

The energy constant in the GAB model (k), the difference between the energy linked to multilayer sorption heat and condensation heat of pure water became minor when k ≤ 1 [65]. All H17@CH hydrogel films had K values of 0≤ k ≤1. CH, H17(100)@CH, H17(130)@CH, and H17(150)@CH had K values of 0.8267±0.087, 0.8748±0.0415, 0.8718±0.0361 and 0.90419±0.0297, respectively (Table 2).

Table 2: GAB of water vapor sorption isotherm models parameters, correlation coefficients, and Chi-square (χ^2)

Parameters	CH	H17(100)@CH	H17(130)@CH	H17(150)@CH
		GAB model		
M_o	1.8705±1.016	1.6372±1.059	1.5742±0.8605	1.2835±1.391
k	0.8267±0.087	0.8748±0.0415	0.8718±0.0361	0.90419±0.0297
C	0.4704±0.430	0.4034±0.404	0.34401±0.1569	0.3390±0.1809
R^2	0.9903	0.9962	0.9972	0.9971
χ^2	3.23×10⁻³	1.21×10⁻³	8.0491×10⁻⁴	7.850×10⁻⁴

For Peleg modeling, the mass transfer rate ($k1$) at the start of the sorption is significantly affected by the rising amounts of H17. With increasing H17 concentration, the Peleg rate constant $k1$ of H17@CH hydrogel films increases. The Peleg rate constant $k1$ of H17@CH hydrogel films increases with increasing H17 content. The mass transfer rate ($k1$) increases from 0.4604±0.0971 to 1.2007±0.1131 h(g/g)⁻¹ compared to CH hydrogel film [0.43813±0.093 h(g/g)⁻¹] as demonstrated in Table (3). For H17@CA films, Peleg capacity constant ($k2$) showed a definite pattern with rising H17 content, but K_2 ((g/g)⁻¹) showed an increasing trend with increasing H17 content. When compared to the control (0.3645±0.143 ((g/g)⁻¹), K_2 fell from 1.0081±0.1141 to 1.1226±0.0891 ((g/g)⁻¹) as mentioned in Table (3).

According to the Smith model, water molecules are adsorbed in two portions. The first fraction, which has a higher condensation heat than pure water, follows the Langmuir model. The second fraction, which arises after the first is adsorbed and is made up of a multilayer of condensed water molecules, prevents the first from evaporating [53].

The Smith model only accounts for the behavior of the second fraction [54, 55].

$$M_c = A + B \ln(1 - a_w) \dots\dots (10)$$

The amount of water in the first sorbed fraction is A, and the amount of water in the multilayer moisture fraction is B.

This equation could be used in the water activity range of 0.5 to 0.95.

The Smith model adequately explained the moisture sorption isotherms of H17@CH hydrogel films. The constants A of this model in this investigation range from 0.05009±0.0193, 0.0454±0.018 and 0.0329±0.0120 which correspond to H17(100)@CH, H17(130)@CH, and H17(150)@CH, respectively, when compared to CH control film of 0.0727±0.036 g/g. The constants B were 0.3857±0.011, 0.3713±0.011 and 0.3577±0.007 of H17(100)@CH, H17(130)@CH, and H17(150)@CH, respectively compared with control sample CH 0.3928±0.022g/g (Table 3).

The actual data meets the model's prediction when the correlation coefficients (R^2) are higher and the Chi-square (χ^2) is lower, implying acceptable fitting. According to R^2 and Chi-square (χ^2), the GAB showed R^2 =0.9903 to 0.9972 and χ^2 = 3.23×10⁻³ to 8.0491×10⁻⁴ (Table 2). Peleg fitting gives R^2 = 0.9959 to 0.9984 and χ^2 =1.82×10⁻³ to 6.38×10⁻⁴ (Table 3). However, Smith modeling showed R^2 =0.9840 to 0.9978 and χ^2 = 1.15×10⁻³ to 4.75×10⁻⁴ (Table 3). All models were accepted to describe the moisture sorption of

H17@CH films based on the definition of an appropriate fitting model.

Table 3: Peleg and Smith modeling of water vapor sorption isotherm parameters, correlation coefficients, and Chi-square (χ^2)

Peleg model				
Parameters	CH	H17(100)@CH	H17(130)@CH	H17(150)@CH
$k1$	0.43813±0.093	0.4604±0.0971	0.4877±0.1208	1.2007±0.1131
$k2$	0.3645±0.143	1.0081±0.1141	1.0171±0.091	1.1226±0.0891
$N1$	4.4659±0.850	0.7024±0.1806	0.8475±0.2283	0.83451±0.2041
$N2$	0.5160±0.2710	5.4971±0.7106	5.8344±1.0126	6.5947±1.0377
R^2	0.9959	0.9984	0.9980	0.9982
χ^2	1.82×10^{-3}	6.45×10^{-4}	7.58×10^{-4}	6.38×10^{-4}
Smith model				
Parameters	CH	H17(100)@CH	H17(130)@CH	H17(150)@CH
A	0.0727±0.036	0.05009±0.0193	0.0454±0.018	0.0329±0.0120
B	-0.3928±0.022	-0.3857±0.011	-0.3713±0.011	-0.3577±0.007
R^2	0.9840	0.9952	0.9951	0.9978
χ^2	4.27×10^{-3}	1.22×10^{-3}	1.15×10^{-3}	4.75×10^{-4}

3.9. Antimicrobial activity
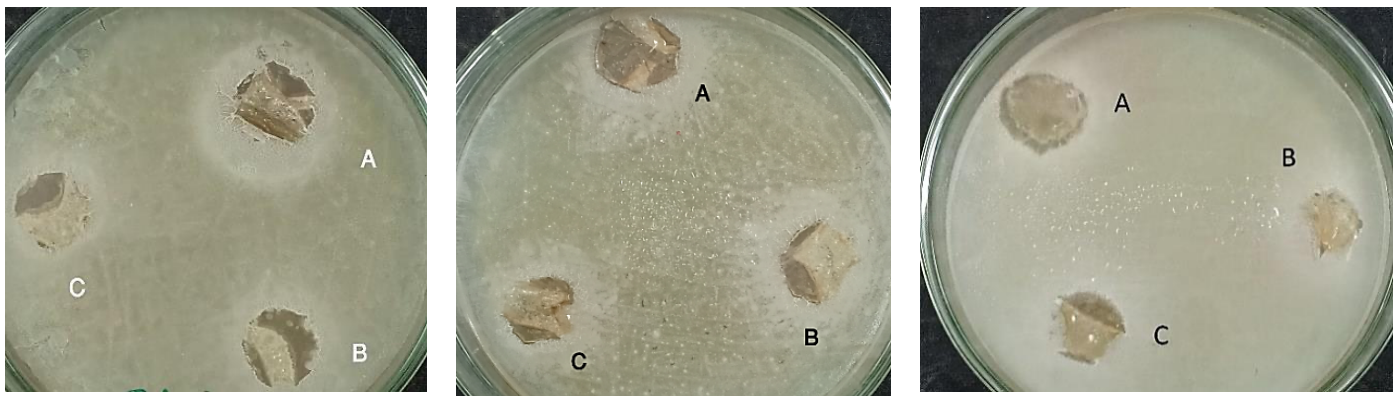
Staphylococcus aureus   *Escherichia coli*   *Candida albicans*

Figure 9: Inhibition zone caused by H17@CH hydrogel film

The antimicrobial activity against food-borne Gram Negative Bacteria: *Escherichia coli* (ATCC 25922), Gram-positive bacteria: *Staphylococcus aureus* (ATCC 6538), and pathogenic yeast *Candida albicans* (ATCC 10231). All films possess significant antimicrobial influence against all tested foodborne microorganisms as shown in Figure (10). H17(150μg)@CH hydrogel film showed the highest inhibition zone of 24±1.0, 22.3±0.57, and 21±1.0 mm, respectively against *Escherichia coli, Staphylococcus aureus* and *Candida albicans*.

With a comparison from the previous study, We discovered that the synthesized form of benzothiazepine is thought to be the basis for new, powerful antibacterial compounds against Gram-positive bacteria and Gram-negative bacteria fungi species [66].

Table 4: Inhibition zone (mm) generated by H17@CH films at different H17 contents

Organism	H17(100)@CH	H17(130)@CH	H17(150)@CH
Escherichia coli	18.3±0.57 [a]	20±1.0 [ab]	24±1.0 [c]
Staphylococcus aureus	17±1.0 [a]	19±1.0 [b]	22.3±0.57 [c]
Candida albicans	17±1.0 [a]	19±1.0 [a]	21±1.0 [b]

a-c: Means with identical letters in each raw signify that there is no statistical difference ($p < 0.05$).

Conclusion

Herein, we have succeeded in fabricating a novel active packaging chitosan hydrogel film (H17@CH) that contains azoloazine derivatives (H17) as a new antimicrobial agent. The films were characterized by ATR-IR, XRD, XPS spectroscopy, and FE-SEM. H17's structure was identified using ^{1}HNMR. H17 showed considerable cell viability and fair cytotoxicity. The antimicrobial component (H17) was added to chitosan with different concentrations (100, 130, and 150μg). H17@CH showed inhibitory action against *Escherichia coli, Staphylococcus aureus,* and *Candida albicans.* The H17(100)@CH showed the maximum swelling ratio was 69.41±3.9 g/g. H17(150)@CH film had the least WVP value (15.60±1.52 g.mm.kPa^{-1}.h^{-1}.m^{-2}) when compared to the control (21.47± 2.0 g.mm.kPa^{-1}.h^{-1}.m^{-2}). GAB, Peleg, and Smith models were agreed to refer to the moisture sorption of H17@CH films. Therefore, the advantages of H17@CH hydrogel film will promote the development of active packaging based on azoloazine derivatives.

References

1. Huang, T., et al., *Polymeric Antimicrobial Food Packaging and Its Applications.* Polymers, 2019. **11**(3).
2. Sultan, M., et al., *Active packaging gelatin films based on chitosan/Arabic gum/coconut oil Pickering nanoemulsions.* Journal of Applied Polymer Science, 2022. **139**(1): p. 51442.
3. Partovi, R., et al., *Antimicrobial Activity of Polylactic Acid Film Incorporated With Marjoram and Clove Essential Oils on Microbial and Chemical Properties of Minced Beef During Refrigerated Storage.* International Journal of Enteric Pathogens, 2020. **8**: p. 25-31.
4. Queirós, L.C.C., et al., *Development of carboxymethyl xylan films with functional properties.* Journal of food science and technology, 2017. **54**(1): p. 9-17.
5. Mironescu, M., et al., *Green Design of Novel Starch-Based Packaging Materials Sustaining Human and Environmental Health.* Polymers, 2021. **13**(8): p. 1190.
6. Irkin, R. and O.K. Esmer, *Novel food packaging systems with natural antimicrobial agents.* Journal of food science and technology, 2015. **52**(10): p. 6095-6111.
7. Quintavalla, S. and L. Vicini, *Antimicrobial food packaging in meat industry.* Meat Science, 2002. **62**(3): p. 373-380.
8. Sultan, M., et al., *Fabrication and evaluation of antimicrobial cellulose/Arabic gum hydrogels as potential drug delivery vehicle.* International Journal of Biological Macromolecules, 2023. **242**: p. 125083.
9. Joerger, R., *Antimicrobial Films for Food Applications: A Quantitative Analysis of Their Effectiveness,".* Packaging Technology and Science, 2007. **20**: p. 231-273.
10. Tohamy, H.-A.S., G. Taha, and M. Sultan, *Dialdehyde cellulose/gelatin hydrogel as a packaging material for manganese oxides adsorbents for wastewater remediation: Characterization and performance evaluation.* International Journal of Biological Macromolecules, 2023. **248**: p. 125931.
11. Mir, S.A., et al., *Effect of plant extracts on the techno-functional properties of biodegradable packaging films.* Trends in Food Science & Technology, 2018. **80**: p. 141-154.
12. Ribeiro-Santos, R., et al., *Use of essential oils in active food packaging: Recent advances and future trends.* Trends in Food Science & Technology, 2017. **61**: p. 132-140.
13. Vimaladevi, S., et al., *Packaging performance of organic acid incorporated chitosan films on dried anchovy (Stolephorus indicus).* Carbohydrate Polymers, 2015. **127**: p. 189-194.
14. Pilevar, Z., et al., *Application of Bacteriocins in Meat and Meat Products: An Update.* Current Nutrition & Food Science, 2018. **14**.
15. Hoseinnejad, M., S.M. Jafari, and I. Katouzian, *Inorganic and metal nanoparticles and their antimicrobial activity in food packaging applications.* Critical Reviews in Microbiology, 2018. **44**(2): p. 161-181.
16. Ramadan, M.A., G.M. Taha, and W.Z.E.L.A. El- Mohr, *Antimicrobial and UV protection finishing of Polysaccharide -Based Textiles using Biopolymer and AgNPs.* Egyptian Journal of Chemistry, 2020. **63**(7): p. 2707-2716.
17. Sultan, M., et al., *Physically-crosslinked hydroxyethyl cellulose-g-poly (acrylic acid-co-acrylamide)-Fe3+/silver nanoparticles for water disinfection and enhanced adsorption of basic methylene blue dye.* International Journal of Biological Macromolecules, 2022. **196**: p. 180-193.
18. Lim, L.-T., *Enzymes for food-packaging applications.* 2015. p. 161-178.
19. Ibrahim, H.M., et al., *Production of Antibacterial Cotton Fabrics via Green*

Treatment with Nontoxic Natural Biopolymer Gelatin. Egyptian Journal of Chemistry, 2019. **62**(Special Issue (Part 2) Innovation in Chemistry): p. 655-669.

20. Ibrahim, H.M., et al., *Enhancing antibacterial action of gauze by adding gelatin nanoparticles loaded with spectinomycin and chloramphenicol.* Cellulose, 2022. **29**(10): p. 5677-5688.

21. Mousavi Khaneghah, A., et al., *Efficacy of Antimicrobial Agents for Food Contact Applications: Biological Activity, Incorporation into Packaging, and Assessment Methods: A Review.* Journal of Food Protection, 2018. **81**(7): p. 1142-1156.

22. Suhr, K.I. and P.V. Nielsen, *Antifungal activity of essential oils evaluated by two different application techniques against rye bread spoilage fungi.* Journal of Applied Microbiology, 2003. **94**(4): p. 665-674.

23. Ahmed, S., et al., *Research progress on antimicrobial materials for food packaging.* Critical Reviews in Food Science and Nutrition, 2020: p. 1-14.

24. Ibrahim, H.M., et al., *Chitosan nanoparticles loaded antibiotics as drug delivery biomaterial.* journal of applied pharmaceutical science, 2015. **5**: p. 085-090.

25. Taha, G.M., et al., *Designing of semiconductive cotton fabrics based on poly (propynyl benzo thiazolone) with UV protection and antibacterial properties.* Materials Science and Engineering: B, 2022. **283**: p. 115857.

26. Baseer, R.A., et al., *Modified cotton fabrics with poly (3-(furan-2-carboamido) propionic acid) and poly (3-(furan-2-carboamido) propionic acid)/gelatin hydrogel for UV protection, antibacterial and electrical properties.* Arabian Journal of Chemistry, 2020. **13**(6): p. 5614-5626.

27. Castro, M., L. Gerschenson, and C. Campos, *Stability of sorbates in the presence of EDTA: Effect of pH, packaging material and sequestrant level.* Journal of the Science of Food and Agriculture, 2005. **85**: p. 328-332.

28. Leelaphiwat, P., et al., *Effects of nisin and EDTA on morphology and properties of thermoplastic starch and PBAT biodegradable films for meat packaging.* Food Chemistry, 2022. **369**: p. 130956.

29. Trinetta, V., et al., *Antifungal Packaging Film to Maintain Quality and Control Postharvest Diseases in Strawberries.* Antibiotics, 2020. **9**(9): p. 618.

30. Li, T., et al., *Development of electrospun films enriched with ethyl lauroyl arginate as novel antimicrobial food packaging materials for fresh strawberry preservation.* Food Control, 2021. **130**: p. 108371.

31. Nguyen Van Long, N., C. Joly, and P. Dantigny, *Active packaging with antifungal activities.* International Journal of Food Microbiology, 2016. **220**: p. 73-90.

32. Maher, H.M., et al., *Quantitative screening of parabens in Ready-to-eat foodstuffs available in the Saudi market using high performance liquid chromatography with photodiode array detection.* Arabian Journal of Chemistry, 2020. **13**(1): p. 2897-2911.

33. Gálvez-Ontiveros, Y., et al., *Presence of Parabens and Bisphenols in Food Commonly Consumed in Spain.* Foods, 2021. **10**(1): p. 92.

34. Narasagoudr, S.S., et al., *Ethyl vanillin incorporated chitosan/poly(vinyl alcohol) active films for food packaging applications.* Carbohydrate Polymers, 2020. **236**: p. 116049.

35. Lin, Q.B., et al., *Analysis of isothiazolinone biocides in paper for food packaging by ultra-high-performance liquid chromatography-tandem mass spectrometry.* Food additives & contaminants. Part A, Chemistry, analysis, control, exposure & risk assessment, 2010. **27**: p. 1775-81.

36. Lin, Q., et al., *Kinetic migration of isothiazolinone biocides from paper packaging to Tenax and Porapak.* Food Additives & Contaminants: Part A, 2011. **28**: p. 1294 - 1301.

37. Heo, J., U.-j. Kim, and J.-E. Oh, *Simultaneous quantitative analysis of four isothiazolinones and 3-iodo-2-propynyl butyl carbamate present in hygienic consumer products.* Environmental Engineering Research, 2018. **24**.

38. Kassem, A., et al., *New azoloazine derivatives as antimicrobial agents: Synthesis under microwave irradiations, structure elucidation, and antimicrobial activity.* Journal of Heterocyclic Chemistry, 2019. **57**.

39. Glomb, T. and P. Świątek, *Antimicrobial Activity of 1,3,4-Oxadiazole Derivatives.* International Journal of Molecular Sciences, 2021. **22**(13).

40. Slater, T.F., B. Sawyer, and U. Sträuli, *Studies on succinate-tetrazolium reductase systems: III. Points of coupling of four different tetrazolium salts III. Points of*

coupling of four different tetrazolium salts. Biochimica et Biophysica Acta, 1963. **77**: p. 383-393.

41. van de Loosdrecht, A.A., et al., *A tetrazolium-based colorimetric MTT assay to quantitate human monocyte mediated cytotoxicity against leukemic cells from cell lines and patients with acute myeloid leukemia.* Journal of Immunological Methods, 1994. **174**(1): p. 311-320.

42. Sultan, M., O.M. Hafez, and M.A. Saleh, *Quality assessment of lemon (Citrus aurantifolia, swingle) coated with self-healed multilayer films based on chitosan/carboxymethyl cellulose under cold storage conditions.* International Journal of Biological Macromolecules, 2022. **200**: p. 12-24.

43. Taha, G.M., E.S. Mansor, and M. Sultan, *Development of Arabic gum-based AgTiO2 nanocomposite hydrogel as high efficient adsorbent of cationic dye methylene blue from water.* International Journal of Biological Macromolecules, 2021. **193**: p. 1859-1870.

44. Sultan, M., et al., *Fabrication of highly efficient nano-composite films based on ZnO-g-C3N4 @ PAA-g-(HEC/PVA)-Fe3+ for removal of methylene blue dye from water.* Journal of Water Process Engineering, 2021. **42**: p. 102184.

45. Sultan, M., A.A. Abdelhakim, and M.A. Nassar, *Cellulose-Based Hydrogels as Smart, Green and Controllable Nitrogenous Fertilizers Releasing Agents.* Journal of Testing and Evaluation, 2019.

46. Sultan, M., et al., *Active packaging of chitosan film modified with basil oil encapsulated in silica nanoparticles as an alternate for plastic packaging materials.* Food Bioscience, 2023. **51**: p. 102298.

47. Moradi, M., et al., *Characterization of antioxidant chitosan film incorporated with Zataria multiflora Boiss essential oil and grape seed extract.* LWT - Food Science and Technology, 2012. **46**(2): p. 477-484.

48. Sultan, M., O.M. Hafez, and M.A. Saleh, *Quality assessment of lemon (Citrus aurantifolia, swingle) coated with self-healed multilayer films based on chitosan/carboxymethyl cellulose under cold storage conditions.* International Journal of Biological Macromolecules, 2021.

49. Ibrahim, S.A. and M. Sultan, *Superhydrophobic Coating Polymer/Silica Nanocomposites: Enhancing Water Vapor Barrier Properties of Packaging Paper with Ultra-Thin PS/silica nanocomposite polymer Coating.* Egyptian Journal of Chemistry, 2019. **62**(1): p. 131-139.

50. van 't Hag, L., et al., *Drying of African leafy vegetables for their effective preservation: the difference in moisture sorption isotherms explained by their microstructure.* Food & Function, 2020. **11**(1): p. 955-964.

51. Peleg, M., *An Empirical Model for the Description of Moisture Sorption Curves.* Journal of Food Science, 2006. **53**: p. 1216-1217.

52. Shafaei, S.M., A.A. Masoumi, and H. Roshan, *Analysis of water absorption of bean and chickpea during soaking using Peleg model.* Journal of the Saudi Society of Agricultural Sciences, 2016. **15**(2): p. 135-144.

53. Andrade P, R.D., R. Lemus M, and C.E. PÉRez C, *MODELS OF SORPTION ISOTHERMS FOR FOOD: USES AND LIMITATIONS.* Vitae, 2011. **18**: p. 325-334.

54. Manshor, N.M., J. Jai, and F. Hamzah, *Moisture sorption of cassava starch film incorporated with kaffir lime oil and the prediction models.* AIP Conference Proceedings, 2021. **2332**(1): p. 020001.

55. Saberi, B., et al., *Water Sorption Isotherm of Pea Starch Edible Films and Prediction Models.* Foods, 2016. **5**(1).

56. van Tonder, A., A.M. Joubert, and A.D. Cromarty, *Limitations of the 3-(4,5-dimethylthiazol-2-yl)-2,5-diphenyl-2H-tetrazolium bromide (MTT) assay when compared to three commonly used cell enumeration assays.* BMC research notes, 2015. **8**: p. 47-47.

57. Maehara, Y., et al., *The ATP assay is more sensitive than the succinate dehydrogenase inhibition test for predicting cell viability.* European Journal of Cancer and Clinical Oncology, 1987. **23**(3): p. 273-276.

58. Gieroba, B., et al., *Spectroscopic studies on the temperature-dependent molecular arrangements in hybrid chitosan/1,3-β-D-glucan polymeric matrices.* International Journal of Biological Macromolecules, 2020. **159**: p. 911-921.

59. Li, P.-C., et al., *Fabrication and Characterization of Chitosan Nanoparticle-Incorporated Quaternized Poly(Vinyl Alcohol) Composite Membranes as Solid Electrolytes for Direct Methanol Alkaline Fuel Cells.* Electrochimica Acta, 2016. **187**: p. 616-628.

60. Omidi, M., A. Yadegari, and L. Tayebi, *Wound dressing application of pH-sensitive*

carbon dots/chitosan hydrogel. RSC Advances, 2017. **7**(18): p. 10638-10649.

61. Zheng, J., et al., *Production of Graphite Chloride and Bromide Using Microwave Sparks.* Scientific Reports, 2012. **2**(1): p. 662.

62. Xu, G., et al., *Biomass-derived porous carbon materials with sulfur and nitrogen dual-doping for energy storage.* Green Chemistry, 2015. **17**(3): p. 1668-1674.

63. Alamri, M.S., et al., *Determination of Moisture Sorption Isotherm of Crosslinked Millet Flour and Oxirane Using GAB and BET.* Journal of Chemistry, 2018. **2018**: p. 2369762.

64. Brunauer, S., P.H. Emmett, and E. Teller, *Adsorption of Gases in Multimolecular Layers.* Journal of the American Chemical Society, 1938. **60**(2): p. 309-319.

65. Enrione, J.I., S.E. Hill, and J.R. Mitchell, *Sorption Behavior of Mixtures of Glycerol and Starch.* Journal of Agricultural and Food Chemistry, 2007. **55**(8): p. 2956-2963.

66. Kassem, A.F., et al., *New azoloazine derivatives as antimicrobial agents: Synthesis under microwave irradiations, structure elucidation, and antimicrobial activity.* Journal of Heterocyclic Chemistry, 2020. **57**(2): p. 611-620.